Authors' accepted manuscript
Article published in *Computers in Biology and Medicine*, vol. 79, p. 45-58 (2016)
http://dx.doi.org/10.1016/j.compbiomed.2016.10.001

A graph-based approach for spatio-temporal segmentation of coronary arteries in X-ray angiographic sequences ☆

Faten M'hiri[a,*], Luc Duong[a], Christian Desrosiers[a], Mohamed Leye[b], Joaquim Miró[b], Mohamed Cheriet[c]

[a] *Department of Software and IT Engineering, École de technologie supérieure, Montreal, Canada*
[b] *Department of Cardiology, Sainte-Justine Hospital, Montreal, Canada*
[c] *Automated Production Engineering, École de technologie supérieure, Montreal, Canada*

Abstract

The segmentation and tracking of coronary arteries (CAs) are critical steps for the computation of biophysical measurements in pediatric interventional cardiology. In the literature, most methods are focused on either segmenting the vessel lumen or on tracking the vessel centerline. However, they do not simultaneously combine the segmentation and tracking of a specific CA. This paper introduces a novel algorithm for CA segmentation and tracking from 2D X-ray angiography sequences. The proposed algorithm is based on the Temporal Vessel Walker (TVW) segmentation method, which combines graph-based formulation and temporal priors. Moreover, superpixel groups are used by TVW as image primitives to ensure a better extraction of the CA. The proposed algorithm, TVW with superpixels (SP-TVW), returns an accurate result to segment and track the artery along the angiogram. Quantitative results over 12 sequences of young patients show the accuracy of the proposed framework. The results return a mean recall of 84% in the dataset. In addition, the proposed method returned a Dice index of 70% in segmenting and tracking right coronary arteries and circumflex arteries.

☆This work was supported by the Fonds de recherche du Quebec Nature et technologies FQRNT (www.fqrnt.gouv.qc.ca) and the Natural Sciences and Engineering Research Council of Canada NSERC (www.nserc-crsng.gc.ca).

*Corresponding author.
Email address: faten.mhiri.1@ens.etsmtl.ca (Faten M'hiri)

The performance of the proposed method surpasses the existing polyline method in tracking the centerline of CA with a more precise localization of the centerline, resulting in a smaller distance error of 0.23mm compared to 0.94mm.

Keywords: Segmentation, Graph-based Method, Tracking, Coronary Arteries, Random Walker, X-ray Angiography, Superpixels

1. Introduction

Two-dimensional (2D) X-ray moving sequences (also called angiograms) are used in percutaneous coronary interventions (PCI) for the diagnosis and treatment of coronary artery (CA) pathologies in newborns and young patients. While other imaging modalities such as computed-tomography are used prior to PCI intervention to have a general view of the CA tree, 2D X-ray angiography allows the visualization of the arteries in real-time during the intervention displaying also the motion of the arteries under respiratory and cardiac work. The accurate and repeatable segmentation and tracking of CAs from 2D angiograms are essential for the assessment of the biophysical measurements of the arteries to predict cardiovascular diseases.

These measurements include computing the vessel segment length [1], detecting stenosis [2] and estimating the severity of a stenosis by measuring the vessel's diameter [3]. Segmenting and tracking the artery along the moving angiography sequence is a key step for measuring the artery and assessing its dynamics in the cardiac cycle.

Vessel segmentation from a 2D moving sequence is a challenging task. First, the visualization of CAs in X-rays depends on the diffusion of the contrast agent in the blood flow. The faster the diffusion of the contrast agent, the harder it is to outline the CA. This is the case for pediatric patients, where the heart rate can be as high as 160 beats per min (twice that of an adult). Therefore, an entire vessel tree cannot be depicted in a single image, but gradually in the angiographic sequence at a typical frame rate of 15 frames/s. It would be more relevant to segment only section of the artery [4], rather than segmenting the whole coronary tree. Moreover, the displacements of CAs are influenced by both the respiratory and cardiac motions. For these reasons, it is difficult to track CAs automatically with these motions. To address this problem, temporal coherence should be preserved, while segmenting one artery in the sequence's frames. This coherence will

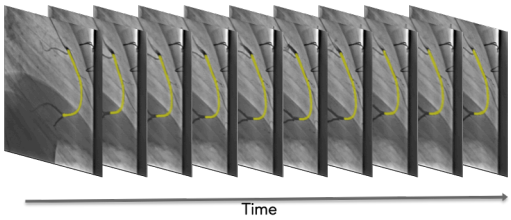

Figure 1: Overview of the segmentation of a coronary artery in 2D+time: Segmenting and tracking the right coronary artery (highlighted in yellow) in an angiographic motion sequence.

guarantee that the method is tracking the specific artery despite the respiratory and cardiac motions. In addition, using new image features to define homogeneous groups of pixels can enhance the segmentation accuracy. Superpixels have been used to define image primitives for image segmentation [5]. They can help by preserving the essential information while simplifying the spatio-temporal segmentation. Instead of extracting pixels independently, the method would extract a group of connected pixels that share the same properties.

Our objective is to design a spatio-temporal segmentation algorithm that can be coherent both spatially and temporally for pediatric interventional cardiology. The spatial coherence guarantees that the method segments one particular vessel from the background, while the temporal coherence tracks the segmented vessel in the motion sequence. The results obtained will guide cardiologists after PCI interventions in evaluating the dynamics and the measurements of the vessel of interest (VOI) during the cardiac cycle.

The contribution of this paper is the development of an algorithm for segmenting and tracking a specific CA in a moving X-ray sequence. Figure 1 illustrates the results of the proposed work, where a specific artery is segmented and tracked in a moving X-ray sequence. This work was previously undertaken in [6]. The previous work introduced a multiscale graph-based method that combines vesselness features with a temporal prior: the multiscale Temporal Vessel Walker (TVW). This study extends the work presented in [6] as follows:

1. It enhances the TVW [6] by incorporating superpixels as image primitives.
2. It uses the SP-TVW method within a multi-size superpixel pipeline, rather than applying the method at different scales of the image. This

indicated to be more efficient than using a multiscale framework [6].
3. No post-processing step is used, unlike the previous work where shape matching is applied for post-processing.
4. While the previous method was tested on only 5 angiographic sequences, in this paper, we evaluated the algorithm on a larger dataset of 12 sequences displaying different types of CAs.

The findings are expected to significantly contribute to the field of segmentation and tracking in 2D X-ray sequences. Most importantly, the findings may lead to the development of new protocols for assessing and evaluating CA dynamics directly from monoplane 2D X-ray sequences.

This paper begins by discussing existing literature on vessel segmentation and tracking. Then, we describe the proposed pipeline for spatio-temporal segmentation. In sections 4 and 5, we show the experimental results on young patients' datasets and discuss these results. In section 6, we summarize our findings by discussing future works.

2. Literature review

Different approaches have been proposed in literature for segmenting CAs. A complete review of segmentation methods can be found in [7]. However, most methods deal with the segmentation of a single image, and not a moving angiogram sequence. To consider the movement of a CA, other studies have suggested a solution for tracking the same structure in time. The polyline tracking method that was proposed by [8] extracts and tracks a CA's centerline in 2D angiographic sequences. The CA's centerline is represented by a set of lines or *polylines*, and each line is retrieved in the sequence. The polyline tracking method is a reference work in the literature [9], and shows successful qualitative results. Moreover, the method is formulated as a minimization problem on a constructed graph, similar to the proposed method. However, to handle respiratory motion and simplify the computations, polyline tracking is applied after a pre-processing step. Otherwise, the computations can be memory intensive and time consuming because the solution relies on finding the shortest path within a large graph in which each node represents a possible line segment of the centerline. Moreover, the polyline representation of a vessel may lead to the loss of curvature information.

Gao and Sundar [9] presented a motion model to track seeds that belong to the CA during the angiography sequence. Nonetheless, their model considers only cardiac motion, and not both cardiac and respiratory displacements.

More recently, the work in [3] presents a spatio-temporal approach to extract and track the CA tree. However, the method tracks the entire tree, and not one artery in particular. It is accepted that tracking one artery is more challenging because all of the arteries in the sequence will share similar features, and it is difficult to automatically distinguish one from the other, while dealing with the artery's motion in time. Besides, the method in [3] computes the vessel lumen at each point in the centerline individually, and does not compute a global segmentation of the lumen.

Finally, while other studies have used spatio-temporal segmentation to track and segment arteries, they either focus on other types of arteries, which do not have the same motion as CA (such as cortical vessels in [10]), or they work on other imaging modalities such as 3D CT scans in [11], where the artery's displacements are not depicted in the same manner as in 2D X-ray angiograms.

To the best of our knowledge, this work is the first to undertake a spatio-temporal segmentation method, where the method tracks the lumen of one specific artery, while being robust to both respiratory and cardiac motions from a monoplane 2D X-ray sequence.

2.1. Superpixel Method

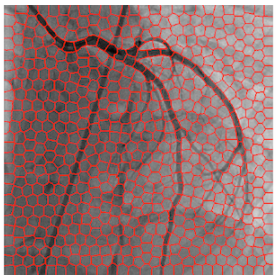

Figure 2: X-ray frame oversegmented with superpixels (red lines are the borders of superpixels)

To enhance the segmentation process, one effective pre-processing step for image representation is superpixel extraction. First introduced by Ren and Malik [5], the method organizes an image into small groups of pixels sharing the same features with low contour energy inside the group. The use of superpixels preserves the important information needed for segmentation, while simplifying the representation of the image and reducing the model's

search space. One of the most efficient methods for superpixel computations is the simple linear iterative clustering (SLIC) [12]. The method performs a local clustering of pixels using their color values and spatial locations. Figure 2 shows an X-ray frame segmented using the SLIC superpixel algorithm [1]. Superpixels have been used within graph-based methods such as normalized cut [13] and random walks [14], where they simplify the graph size and the retrieval of the optimal solution.

3. Proposed method: Temporal segmentation of CA in 2D X-ray moving sequences

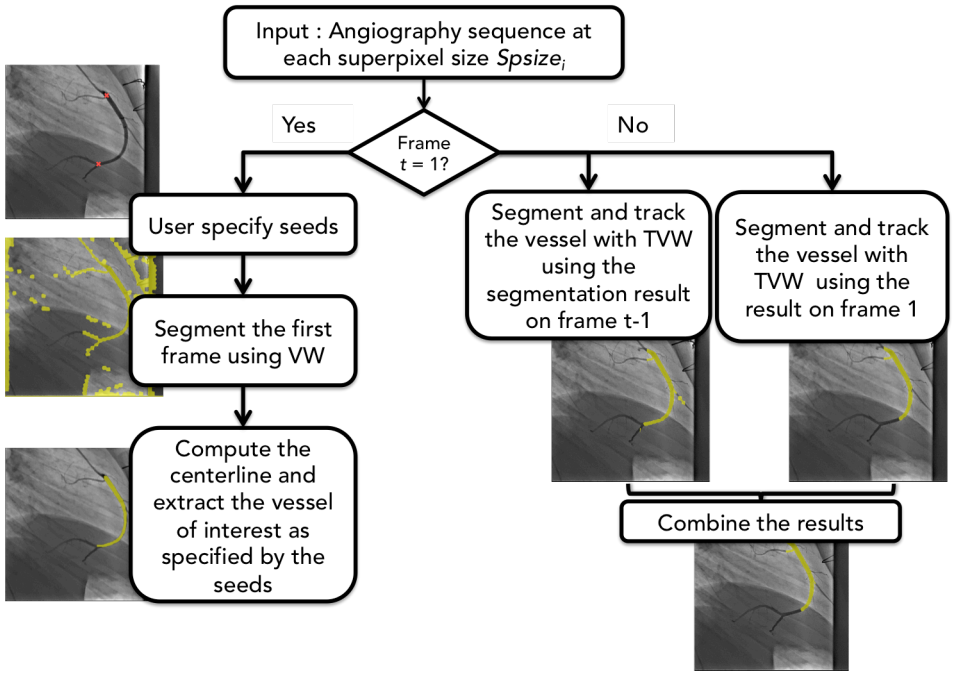

Figure 3: Proposed pipeline for spatio-temporal segmentation of an artery in 2D X-ray angiogram.

Figure 3 illustrates the steps of the proposed algorithm employed for the segmentation and tracking of CAs. At the beginning of the sequence, the

[1] We used the implementation of SLIC from the VLFeat package : http://www.vlfeat.org/api/slic.htm

clinician defines the vessel of interest by specifying -using a simple click- the limits of the vessel. The vessel walker method (VW) [15] with superpixels is applied to segment all the vessels in the image. This result is further refined to extract only the vessel of interest based on the selected seeds, as described in section 3.2.1. For the rest of the sequence, the original Temporal Vessel Walker with superpixels (SP-TVW) is applied, and is described in section 3.2.2. To track and segment the vessel, the method uses the segmentation result at the first frame of the sequence and the segmentation result at the previous frame. The steps presented in Figure 3 are applied for different superpixel sizes to capture large and thinner parts of the artery. The results computed for different superpixel sizes are merged using a weighted combination to obtain a final segmentation result. All of these steps are detailed in the following section. First, we start by presenting the Temporal Vessel Walker model and then all the steps of the new pipeline are described.

3.1. Temporal Vessel Walker

To solve the spatio-temporal segmentation task, the proposed solution is based on the Temporal Vessel Walker method introduced in [6]. The proposed method adapts the random-walks formulation [16], [17] for vessel segmentation in 2D X-ray images. The method adds a temporal prior to preserve the structure of interest. In a multiple-frame sequence where we observe the same vessel of interest, the aim is to segment the vessel from a new frame $\mathcal{I}^t$ at time t, knowing the segmentation result in its previous frame $\mathcal{I}^{t-1}$ (Figure 1).

The proposed idea is as follows: If we have a pixel p_i^{t-1} at location i in $\mathcal{I}^{t-1}$ and p_j^t at the same location in $\mathcal{I}^t$, and if p_i^t or one of its neighbors shares the same features as p_i^{t-1}, then pixel p_j^t or one of its neighbors has a high probability of having the same label (i.e., background or foreground label) as p_i^{t-1}. To guarantee this temporal similarity, we define graph G_τ, which connects by an edge each pixel p_i^{t-1} in $\mathcal{I}^{t-1}$ to a pixel p_j^t and its neighbors within a radius r_τ from $\mathcal{I}^t$, as shown in Figure 4. Each edge has a weight w_{ij}^τ expressing the temporal similarity between p_i^{t-1} and p_j^t:

$$w_{ij}^\tau = \begin{cases} \exp\left\{ -\gamma_\tau \left(I_i^{t-1} - I_j^t\right)^2 \right\}, & \text{if } i = j \\ & \text{or } \mathrm{dist}(i,j) \leq r_\tau \\ 0, & \text{otherwise.} \end{cases} \quad (1)$$

I_i^{t-1} is the intensity value at pixel p_i^{t-1}, and γ_τ is a parameter controlling the effect of the intensity differences on the weight.

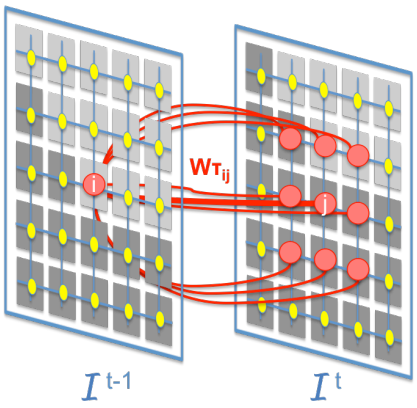

Figure 4: Representation of the temporal graph G_τ: Node i from image $\mathcal{I}^{t-1}$ is connected to the node having the same location in $\mathcal{I}^t$ and its surrounding 8-neighbours. We compute the temporal similarity measures between i and all the connected nodes (j and its neighbors).

We define the TVW following a Bayesian approach. The proposed method looks for a mapping $\boldsymbol{f} : \mathcal{I} \rightarrow \{0, 1\}$, where $f_i = 1$ if the pixel i belongs to the vessel, and $f_i = 0$ if i belongs to the background. Having the image's features (represented by vector Y) and a prior segmentation mask ($\boldsymbol{f}^{t-1}$), the mapping should maximize the posterior probability of the Markov random field (MRF) associated with the label map:

$$\begin{aligned} X^* &= \arg\max_X \; p(X \,|\, Y, X^{t-1}) \\ &= \arg\max_X \; \log p(X) \; + \; \log p(Y \,|\, X) \; + \; \log p(X^{t-1} \,|\, X). \end{aligned} \tag{2}$$

Assuming the pixel features to be conditionally independent given their label, the likelihood term can be defined as

$$\log p(Y \,|\, X) \; = \; \sum_{i=1}^{|\mathcal{I}|} x_i \log p(y_i \,|\, x_i = 1) \; + \; (1 - x_i) \log p(y_i \,|\, x_i = 0). \tag{3}$$

While various image features could be used, such as pixel intensity values and gradient directions, we found that vesselness values were most robust to contrast changes and artery movement. In our method, y_i thus corresponds to the vesselness of pixel i obtained from a Frangi filter [18] and normalized to the $[0, 1]$ interval. Based on an empirical analysis, we observed that the

vesselness values in the arteries (i.e., foreground region) roughly follow a one-sided Laplace distribution, where most pixels have a vesselness near 1, and the probability decreases sharply to zero for smaller values of vesselness. Likewise, the probability of having a near zero vesselness in the background is high, and drops quickly for higher values of vesselness. Using this observation, we model the likelihood of foreground/background pixels as:

$$\begin{aligned} \log p(y_i \,|\, x_i = 1) &\propto -\alpha(1 - y_i) \\ \log p(y_i \,|\, x_i = 0) &\propto -\beta y_i, \end{aligned} \tag{4}$$

where α and β correspond to the scale parameter of their respective Laplace distribution, and are used to control the trade-off between false-positives and false-negatives. For the label image prior, we use the standard Potts model to enforce spatial consistency of labels:

$$\log p(X) \;\propto\; -\sum_{i=1}^{|\mathcal{I}|}\sum_{i=1}^{|\mathcal{I}|} w_{ij}\,|x_i - x_j|. \tag{5}$$

A similar model is used to model the temporal prior of labels:

$$\log p(X^{t-1} \,|\, X) \;\propto\; -\sum_{i=1}^{|\mathcal{I}|}\sum_{j=1}^{|\mathcal{I}|} w^{\tau}_{ij}\,|x_i - x^{t-1}_j|. \tag{6}$$

Combining these definitions, we can then formulate the maximum a posteri (MAP) problem as the task of minimizing the following energy function:

$$\begin{aligned} E(X) \;= \alpha \sum_{i=1}^{|\mathcal{I}|}(1 - y_i)x_i \;+\; \beta \sum_{i=1}^{|\mathcal{I}|} y_i(x_i - 1) \\ +\; \sum_{i=1}^{|\mathcal{I}|}\sum_{j=1}^{|\mathcal{I}|} w_{ij}\,|x_i - x_j| \;+\; \mu \sum_{i=1}^{|\mathcal{I}|}\sum_{j=1}^{|\mathcal{I}|} w^{\tau}_{ij}\,|x_i - x^{t-1}_j|, \end{aligned} \tag{7}$$

where parameter μ is added to control the trade-off between spatial and temporal smoothness.

This formulation corresponds to a graph-cut problem, which can be solved efficiently using a max-flow algorithm. However, because the are susceptible to the shrinking bias problem, graph-cut methods are not well suited for the segmented of thin structures like arteries [19]. Instead, we use a random-walk

approach in which the intergrality constraints on x_i are relaxed to the $[0, 1]$ interval, and the energy function reformulated as follows:

$$\begin{aligned} E(X) \; &= \alpha \sum_{i=1}^{|\mathcal{I}|} (1 - y_i) x_i^2 \; + \; \beta \sum_{i=1}^{|\mathcal{I}|} y_i (x_i - 1)^2 \\ &+ \; \sum_{i=1}^{|\mathcal{I}|} \sum_{j=1}^{|\mathcal{I}|} w_{ij} \, (x_i - x_j)^2 \; + \; \mu \sum_{i=1}^{|\mathcal{I}|} \sum_{j=1}^{|\mathcal{I}|} w_{ij}^{\tau} \, (x_i - x_j^{t-1})^2. \end{aligned} \tag{8}$$

The solution to this quadratic problem can be obtained efficiently by solving a sparse linear system.

The resulting X vector describes the probability for each pixel to belong to the foreground. To obtain a binary segmentation, a threshold has to be selected or computed. We chose Otsu's thresholding algorithm [20] to find a final binary segmentation of X. This well-performing method computes the threshold that minimizes the weighted within-class variance.

The application of TVW alone may succeed in extracting parts of the CA and tracking it in the sequence. Nevertheless, in the context of CA segmentation and tracking, using the Temporal Vessel Walker alone is not sufficient to capture cardiac and respiratory motions of CAs. Therefore, additional steps are necessary to enhance the result of TVW. For this reason, we adapted the method to the CA motion by grouping similar pixels and tracking these groups. To achieve this, superpixels can be an accurate grouping method. In the following section, we present the proposed algorithm for spatio-temporal tracking using the temporal vessel walker with superpixels to segment and track a CA in a 2D X-ray angiogram.

3.2. Temporal Vessel Walker with superpixels for segmentation and tracking

3.2.1. Segmentation of the first frame: Vessel Walker method using superpixels

At the beginning of the X-ray sequence, and because we do not have an initial prior, the method starts by asking the operator (the cardiologist) to specify two seed points. These seeds correspond to the beginning and the end of the vessel of interest, as shown in the first image in Figure 5. More than two seeds can be defined in the case when the contrast in the image is limited, or if there is vessel overlap or many bifurcations. Using the Vessel Walker and the specified seeds, the method extracts the vessel of interest.

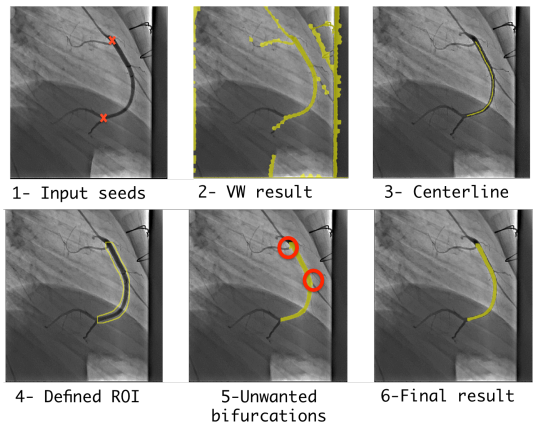

Figure 5: Steps for the segmentation of the first frame.

It is important to accurately extract the lumen of the first frame in the sequence, which is why different steps are used, as shown in Figure 5:

1. Extending the Vessel Walker method using superpixels: The Vessel walker method [15] is applied on the first image of the sequence by using superpixels grouping. The image $\mathcal{I}$ is represented by an undirected graph G. Each by node v_i in G corresponds tp a superpixel sp_i from $\mathcal{I}$. The weight w_{ij} describes mean intensity similarity between two neighbouring nodes v_i to v_j. As shown in the second image in Figure 5, the result extracts all the vessel-like structures in a frame. To extract only the VOI as specified by the seeds, the following steps are needed.
2. Computing the centerline of the VOI: The centerline is computed as the shortest path that connects the endpoints of the vessel (i.e., selected seeds) passing by pixels with similar features. An adjacency matrix is defined to describe the image as a connected graph. Intensity and orientation features are used following the idea in [21]. Using the adjacency matrix and the seed locations, Dijikstra's shortest path algorithm [22] computes the centerline of the vessel (Figure 5).
3. Extracting the lumen of the computed centerline: A region surrounding the computed centerline is defined (the radius of the region is selected empirically) and the lumen within that region is extracted (fourth image in Figure 5). This result may include some bifurcations of the vessel that are not of interest to clinicians (fifth image in Figure 5). A postprocessing step is added to compare the centerline features with

the extracted lumen, keeping only pixels that are similar to the ones in the centerline. The final result is shown in the last image in Figure 5.

While computing the lumen at the first frame may seem to be demanding in terms of the number of steps and computations, the complete computation takes a mean time value of 20 s per frame (running non-optimized Matlab code on an Intel Core i7 3.1 GHz).

3.2.2. Segmentation and tracking: Temporal Vessel Walker using superpixels (SP-TVW)

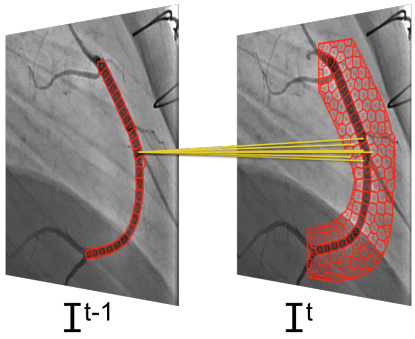

Figure 6: The temporal adjacency matrix computes similarities between the selected source nodes (red points in $\mathcal{I}^{t-1}$) and sink nodes (red points in $\mathcal{I}^{t}$)

The model in Eq.(8) is extended using superpixels. These groups of pixels increase the accuracy of the retrieval of similar groups from one frame to the next. The temporal adjacency matrix w^{τ} defined in Eq.(1) is then modified to use superpixels[2].

The value of w_{ij}^{τ} describes the mean intensity similarity between the superpixels belonging to frame $\mathcal{I}^{t-1}$, (which represent source nodes), and the ones that belong to $\mathcal{I}^{t}$ (the sink nodes).

Because the motion from $\mathcal{I}^{t-1}$ to $\mathcal{I}^{t}$ is located around a specific region, we simplify the computations in the equation (1) by selecting only the superpixels in $\mathcal{I}^{t-1}$ and $\mathcal{I}^{t}$ within a specific region (instead of using all the superpixels in $\mathcal{I}^{t-1}$ and $\mathcal{I}^{t}$). Therefore, the only selected source nodes are the superpixels

[2]Adjacency matrix was computed with the code for the region adjacency graph (source: http://www.mathworks.com/matlabcentral/fileexchange/16938-region-adjacency-graph–rag-)

belonging to the foreground segmentation result in $\mathcal{I}^{t-1}$, and the sink nodes in frame $\mathcal{I}^t$ are those belonging to a specific region of interest ROI_τ, which is the region surrounding the foreground result at $\mathcal{I}^{t-1}$, where the radius of the ROI_τ is selected based on the maximum displacement of arteries from one frame to the next. The temporal adjacency matrix is computed using the selected source and sink nodes, as defined in Figure 6. Considering only these specific nodes gives a sparse adjacency matrix, which speeds up the computations and limits the background noise.

3.3. Proposed algorithm

Algorithm 1 Proposed algorithm for tracking and segmenting coronary arteries in 2D X-ray sequences.

Require: 2D xray sequence of $frame_i$; $i = 1...nbFrm$
Require: The weight assigned to each superpixel size k_j ; $j = 1..SPsize_{Max}$
  for each $frame_i \leftarrow 1, nbFrm$ **do**
    if $frame_i := 1$ **then**
      Ask operator to select seeds (limits of the vessel) ;
      Apply Vessel Walker segmentation with superpixel ;
      Compute the centerline and lumen using the VW result ;
      $TVW_1 \leftarrow$ the computed lumen ;
    else
      for $SPsize_j \leftarrow 1, SPsize_{Max}$ **do**
        $TVW_{(i,i-1)} \leftarrow$ compute SP-TVW using the result at $frame_{i-1}$;
        $TVW_{(i,1)} \leftarrow$ compute SP-TVW using the result at $frame_1$;
        $TVWsize_j = TVW_{(i,i-1)} + 2 \times TVW_{(i,1)}$;
        $TVW_i = TVW_i + k_j \times TVWsize_j$;
      end for
      Threshold the result : $TVW_i^* = TVW_i > mean(TVW_i)$;
    end if
  end for
  RESULT : Segmentation result TVW_i^* of the angiographic sequence ; $i = 1...nbFrm$.

Algorithm 3.3 summarizes the proposed pipeline (as illustrated in Figure 3) for a spatio-temporal segmentation of 2D xray angiography sequence. At the first frame ($frame_i = 1$), the operator (the cardiologist) specifies the artery of interest. The centerline of the artery is computed and then its

lumen is segmented using the vessel walker method. Then, for the rest of the sequence, the algorithm applies the SP-TVW method at different superpixel sizes (where $SPsize_j = [1...SPsize_{Max}]$) to track and segment the same artery in the angiographic sequence.

For each frame i, and at each superpixel size $SPsize_j$, the algorithm computes the temporal vessel walker, using the segmentation result obtained from the previous frame ($TVW_{(i,i-1)}$), and again using the result at the first frame ($TVW_{(i,1)}$). The computations use the segmentation mask of the previous frame because the changes from the previous to the actual frame are less dramatic. Besides, the changes in intensity from consecutive frames are less important. However, during segmentation in the moving sequence, the result from the previous frame may contain some errors (such as overlapping vessels or missing parts of the VOI). Therefore, in addition to the previous frame, the SP-TVW is applied using the first-frame segmentation mask as a prior because this prior was computed accurately: Indeed, the segmentation at the first frame should be validated qualitatively before launching the segmentation for the rest of the sequence (as explained in section 3.2.1). Consequently, both SP-TVW results (i.e., using the previous frame and first frame) are combined to determine the final segmentation result $TVWsize_j$, computed at a specific superpixel size.

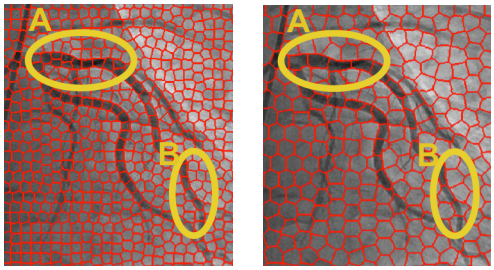

Figure 7: Computing superpixels at different sizes: left: SPsize=20 ; right: SPsize=13.

Because the CA's thickness changes from the proximal to the distal parts of the artery, the result is applied at different superpixel sizes ($SPsize_j = 1..SPsize_{Max}$). Figure 7 shows the superpixels computed at different sizes. We notice that a large SPsize captures the proximal and thick parts of the artery (highlighted region A in Figure 7), which have a high contrast with the background. On the other hand, a smaller SPsize captures the distal thinner parts of the artery, where the contrast level is limited (highlighted

region B in Figure 7). For this reason, the segmentation result $VWTsize_j$ is computed at different superpixel sizes.

The results for the same frame at different superpixel sizes are weighted and combined to obtain a final segmentation result VWT_i at frame i: as the SPsize value decreases, more weight is given to the corresponding TVW result (i.e., the value of k_j increases). To obtain a binary segmentation mask, TVW_i is thresholded. Once the segmentation mask TVW_i^* is obtained, the method uses it to compute the segmentation result VWT_{i+1} in the next frame in the sequence, until the end of the sequence.

4. Experimental results

4.1. Data Acquisition

To evaluate the proposed work, we used a dataset of 12 angiographic sequences of coronary catheterization. The sequences were acquired from six young patients with congenital heart disease from the Sainte-Justine's Hospital (Montreal, Canada). These data were saved and anonymized into the DICOM format, and were recorded after approval by the Sainte-Justine's Institutional Ethics Review Board. The angiograms were acquired by a C-arm Infinix-CFI BP by Toshiba profiling: six angiograms of right coronary arteries (RCA), three angiograms of the left anterior descending artery (LAD), and three others of the circumflex branch (Cx). Each sequence comprised nine frames (± 2) having a size of 512×512 pixels, and each of which represents a single cardiac cycle selected as the one that best delineates the anatomy from among the full angiographic acquisition. Different artifacts are present in our database: The frame-rate is low (15 frames per second), which makes the motion from one frame to the following more pronounced. In addition, some sequences depict sternal sutures (when the patient has been previously operated on), which are dark tubular regions that can alter the segmentation result.

Because it can be complex and time-consuming to manually segment all of the sequence's frames, one segmentation expert (the first author) has manually segmented 4 keyframes for each sequence. Each keyframe represents a different stage of the cardiac cycle: at the beginning (0%), at 20%, at 40%, and at the end of the cycle (100%). Using these frames, it is sufficient to evaluate the performance of the segmentation method because each frame represents different motion changes along the sequence. Only the main vessels were segmented. The manual segmentation is delimited at a terminal

	Observer 1	Observer 2	Observer 3	Ground truth
Observer 1	1.00	0.91	0.87	0.90
Observer 2	0.91	1.00	0.89	0.86
Observer 3	0.87	0.89	1.00	0.87
Ground truth	0.90	0.86	0.87	1.00

Table 1: Cohen's kappa coefficient computed between each pair of observer's manual segmentation.

bifurcation or when the vessel would measure half of its original diameter. This ground-truth data has been subject to a double correction and validation by two cardiologists (the 4th and 5th authors).

Vessel lumen's segmentation is evaluated using the ROC curve's AUC, precision, recall, and Dice metrics. To evaluate the centerline extraction and tracking, we modified the classical computations of precision and recall metrics. PrecisionCL, RecallCL, and the distance error were computed as proposed in [23]: for each pixel in the ground-truth, we checked within its neighborhood of radius 5 if there is a corresponding point from the computed centerline. Finally, we computed the location error between the ground-truth and the computed result to evaluate the accuracy of the centerline location.

4.2. Inter-observer evaluation

Groundtruth data were defined manually. To quantify agreement between manual segmentation results, we asked three trained operators to manually segment the LAD in four frames from one sequence (sequence 1 of our dataset). Each operator was asked to segment the main artery until a terminal bifurcation has been reached or until the diameter of the vessel measures half of its original diameter. All three operators have blindly segmented the LAD, without seeing each others results or the ground truth. Pairwise inter-observer agreements were measured using Cohens Kappa coefficients and are shown in table 1. When we compare the results of the same observer, kappa coefficient is 1 meaning total agreement, which is normal since we compare the same results to each others. Otherwise, the coefficient is between 0.86 and 0.91. This is considered as almost perfect agreement [24] and indicates a low inter-observer variability.

	Polyline tracking	Ours
PrecisionCL	0.78	0.81
RecallCL	0.75	0.78
Distance error	0.94	0.23

Table 2: Average performance of the polyline tracking method [8] versus our proposed algorithm on the 12-sequence dataset in terms of centerline extraction and tracking.

4.3. Comparing the proposed method to polyline tracking

Because the polyline tracking follows only the centerline of the vessel, and our work tracks the lumen of the vessel, both methods are evaluated in terms of centerline tracking and not lumen tracking. To do so, we applied the Hamilton-Jacobi skeletonization method [25] to extract the centerline from our SP-TVW lumen. The Hamilton-Jacobi method analyses the normalized flux of the gradient vector field to detect the centerline points. It has been proven to be computationally efficient and robust to boundary noise. Both the polyline and the proposed methods were initialized using the same centerline computed from the first frame (as described in section 3.2.1) and they were both tested on the 12 angiographic datasets.

Table 2 displays the performance of the polyline tracking method [8] and our algorithm on the dataset. The results are evaluated in terms of the centerline precision (PrecisionCL), and recall (RecallCL), and distance error. The proposed method has a higher trade-off than polyline tracking in terms of PrecisionCL and RecallCL. Moreover, its corresponding distance error of $0.23mm$ is lower than that obtained using polyline tracking, which returns a mean distance error of $0.94mm$.

Fig. 8 shows the centerline extraction performance using the proposed method and the polyline tracking method on sequence 8 of our dataset. Polyline tracking preserves the general shape of the initialized artery. However, as the artery expands because of the cardiac work, polyline tracking cannot capture some parts of the artery, unlike our results. Indeed, the images in the first row in Fig.8 display green colored pixels that exhibit false negatives generated by the polyline tracking approach. The proposed algorithm gives more accurate results and retrieves the CA in the rest of the sequence with fewer false negatives, as shown in the second row of Fig.8. Moreover, despite the presence of false positives in the proposed result (pink pixels), the proposed method overlaps more with the ground-truth compared to the polyline method. As a matter of fact, the location of the computed centerline is well

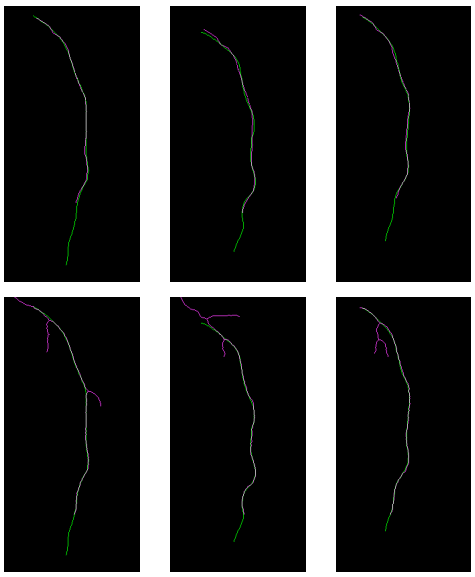

Figure 8: Computed centerline at different frames (left to right: frame 2, 4 and 9) on sequence 8 and their overlap on the ground-truth centerline. Top row: Polyline Tracking results. Bottom row: Our results. Green colored pixels show false negative; pink colored pixels show false positives and white colored pixels are for true positives (i.e., overlap).

aligned with the ground-truth data. This is illustrated by the presence of more white pixels in the proposed results than in the polyline result in Fig.8.

4.4. Extending the TVW model using superpixels: contribution of the proposed algorithm

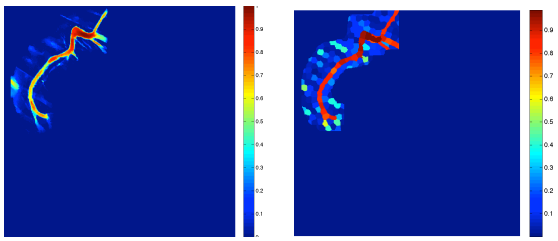

Figure 9: Results showing per-pixel probability values to belong to the foreground, as computed using the TVW without superpixels (left) and with superpixels (right)

Table 3 displays the mean results on four angiographic sequences of our database using the temporal vessel walker (SP-TVW) with superpixels in

	TVW	TVW(multiscale)	SP-TVW
Precision	58.75%	85%	79.75 %
Recall	82%	52.75%	73.5 %
Dice	63.25%	63.5%	75.5 %

Table 3: Average performance (Precision, Recall, and Dice coefficient) on the first four angiographic sequences of our database.

comparison to using TVW pixelwise and to the TVW within the multiscale approach[6]. Using the TVW method pixelwise, while we have a better recall value of 82%, there is limited precision. The TVW within the multiscale approach returns the highest precision result of 85%, but it yields low recall values. On the other hand, TVW with superpixels returns the highest trade-off between recall and precision values, and the highest Dice value of 75.5%.

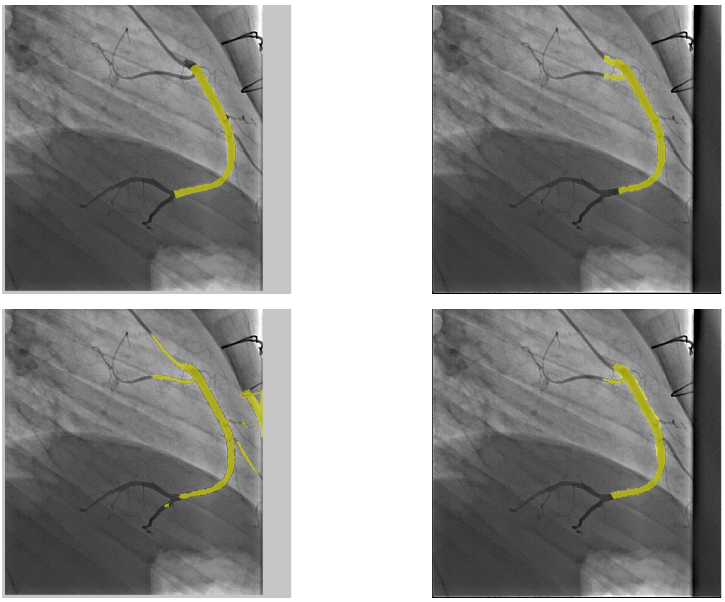

Figure 10: Segmentation overlaid on the original frame 4 of the RCA sequence 3 of our dataset. Top row: the ground-truth (left) and the TVW with superpixels result (right). Bottom row: TVW method pixelwise (left) and TVW within the multiscale approach (right).

Fig. 9 illustrates the computed probabilities of pixels belonging to the foreground (i.e., the non-thresholded results computed using Eq. (8)), using

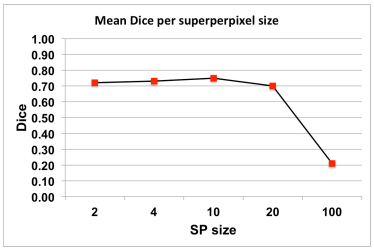

(a) Dice

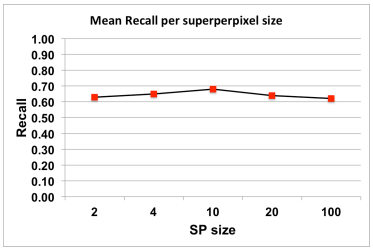

(b) Recall

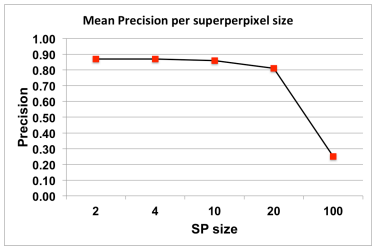

(c) Precision

Figure 11: Influence of the superpixel size on Dice, Recall, and Precision using our proposed work.

the TVW formulation with and without superpixels. The colors in the images shows the probability values; the red pixels correspond to probability that it belongs to the foreground close to 1, while the blue pixels correspond to a probability of 0. The use of superpixels better highlights the difference between the foreground and background regions, whereas the result computed without superpixels has some limitations in terms of extracting parts of the vessels. This is observed particularly in the yellow region at the end of the vessel, where the probability values are around 0.6 and 0.5.

Figure 10 shows the ground-truth and the segmentation results obtained using the three approaches in sequence 3 of our dataset at frame 4. In the left image of the second row, the use of TVW pixelwise displays false positives in its segmentation mask, where sternal sutures belonging to the background are highlighted as part of the artery. SP-TVW and the multiscale approach exhibit more precise results in the extraction of the artery. Nonetheless, the multiscale approach is less precise around the borders of the vessels, where its segmentation mask oversteps the edges of the vessel.

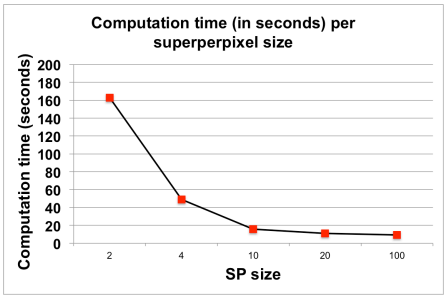

Figure 12: Influence of the superpixel on the computation times per frame.

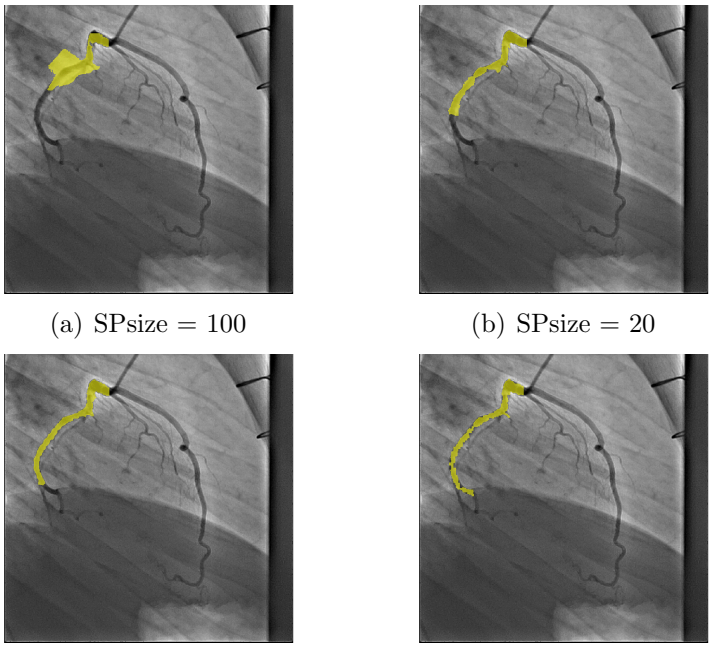

(a) SPsize = 100 (b) SPsize = 20

(c) SPsize = 10 (d) SPsize = 4

Figure 13: Influence of the superpixel using the VWTSP model at different superpixel sizes on the segmentation result.

4.5. Parameter's influence

4.5.1. Superpixel size

In this section, we evaluate the effect of the superpixel size (SPsize) on the mean performance, as illustrated in Fig.11. The values were computed on the first three sequences of the dataset. When the SPsize becomes too large, each superpixel will regroup pixels that are less similar to each other.

This explains the sensitivity of the precision curve when the superpixel size becomes larger than 10. On the other hand, recall values increase as the SPsize is increased, until it reaches the value of SPsize= 10 pixels.

Figure 12 shows the impact of the size of superpixels on the computation times. Note that as the superpixels size increases, the computation times are faster. As the size becomes larger, the number of nodes in the adjacency and temporal adjacency graphs decreases, making the matrices computation lighter.

Finally, Figure 13 displays the impact of different superpixel sizes (from the largest 100 to the smallest 4) on the segmentation result. We can see that as the SPsize gets smaller, fewer errors are made. However, when the SP size is the smallest, there is some difficulty highlighting the border of the vessel.

4.5.2. Tracking parameter μ

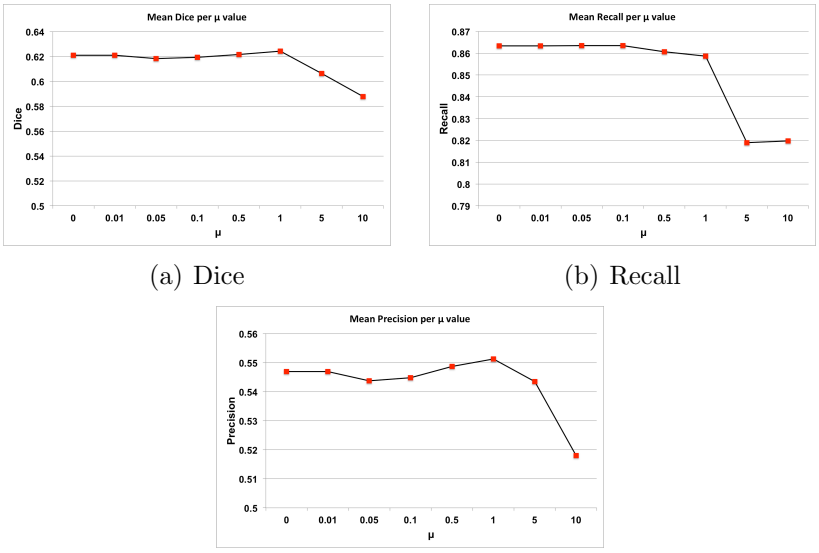

(a) Dice (b) Recall

(c) Precision

Figure 14: Influence of the μ values on the Dice, Recall, and Precision using the TVW method.

Figure 14 shows the influence of the temporal parameter μ on our method. We tested only the TVW using the previous segmentation frame as a prior and at one superpixel size. These tests were done on the first three sequences

of the dataset. The first curve in Figure 14 displays the performance in terms of the Dice values as μ increases. When the μ value is between 0.1 and 1, the Dice curve increases and reaches a peak at $\mu = 1$. Once $\mu > 1$, the performance drops dramatically. Optimal values for the temporal parameter μ are within the interval $[0.1, 1]$. This temporal parameter can have a critical impact on the performance because it helps to ensure that the VOI is tracked along the angiography sequence. Parameter μ has the same effect on the precision curve where the optimal value of μ is within the interval $[0.5, 1]$. However, the parameter does not affect the recall values (as shown in the second curve in Figure 14). Having a temporal prior may limit the rate of false positives, but it can also limit the true positive rate; hence, μ increases the precision level but can also limit the recall value.

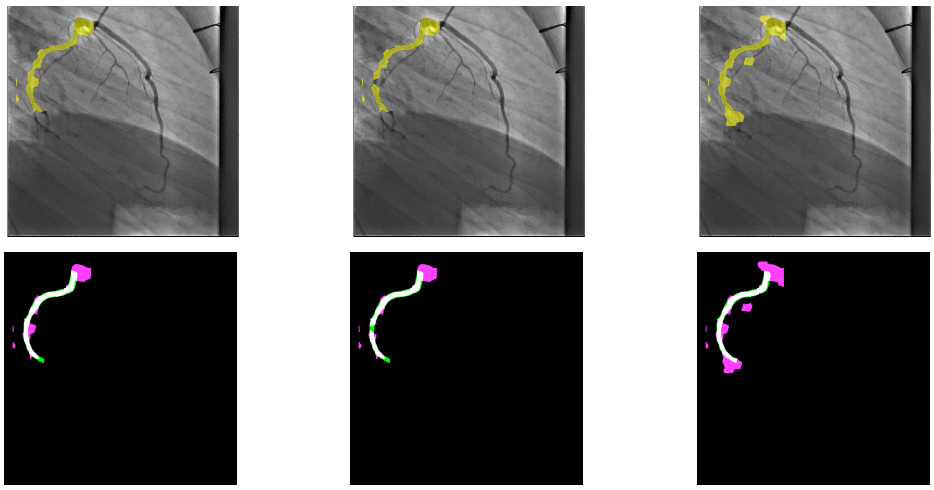

Figure 15: Influence of the μ values on the SP-TVW results: first row: segmentation masks overlaid in yellow on original frames. Bottom row: Segmentation mask displaying true positives (white), false positives (pink), and false negatives (green). From left to right: results at $\mu = 0$, 1, and 10

Figure 15 displays the proposed method's results on the second frame of sequence 2 of our dataset. Each column shows the result for $\mu = 0$, 1, and $\mu = 10$. The top row shows the effect of μ on the segmentation masks. There is some improvement between $\mu = 0$ and $\mu = 1$, where the background noise around the end of the vessel is limited at $\mu = 1$. However, when μ gets a higher value, more background noise is added because the SP-TVW highlights the connection between the previous segmentation result and the actual frame.

These findings are highlighted further in the second row in Figure 15, where it exhibits the overlap between the segmentation mask and the ground-truth: false positive pixels are colored in pink, false negatives in green, and true positives are in white. When parameter $\mu = 1$, false positives are limited compared to the result at $\mu = 0$. On the other hand, when $\mu = 10$, the true positive rate increases and more pixels are colored in white. However, the method becomes less robust to the background noise.

4.5.3. Influence of parameters α and β

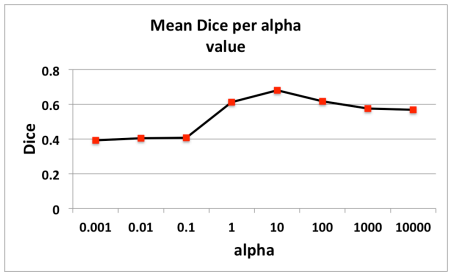

(a) α influence on Dice

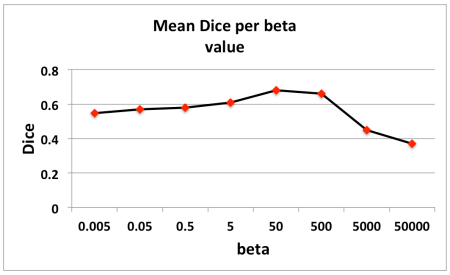

(b) β influence on Dice

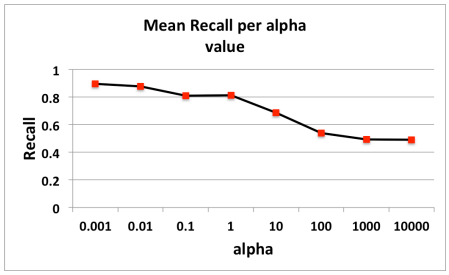

(c) α influence on recall

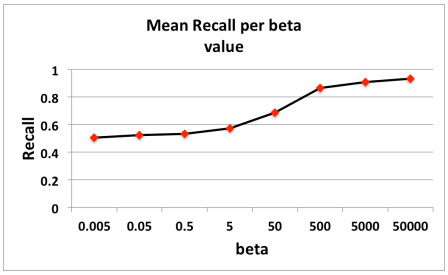

(d) β influence on recall

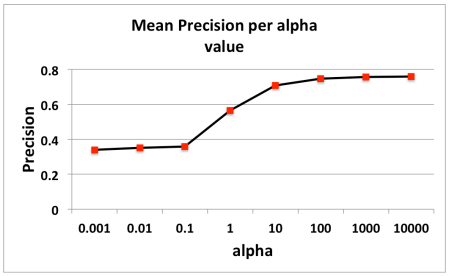

(e) α influence on precision

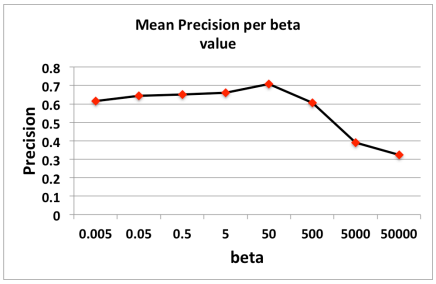

(f) β influence on precision

Figure 16: Influence of α (left column) and β (right column) parameters on Dice, recall, and precision (From top to bottom) using the proposed method.

The impact of parameters α and β, from equation (8), is presented in Figure 16. Parameter α influences the weight of the foreground pixels. As the value of α increases, the more robust becomes the result to background noise, increasing the precision value. On the other hand, when α is greater than 10, the method will discriminate not only background noise, but also the pixels belonging to the vessels, which explains the low recall values. The value of α should be optimally selected to preserve a trade-off between precision and recall. The Dice curve shows that an optimal value of $\alpha = 10$ leads to this trade-off. The parameter β affects the weight of the background pixels. Unlike parameter α, higher β values result in a higher recall. However, background pixels that have an important vesselness value will be considered as part of the foreground. This limits the precision of the method. The Dice curve shows that at $\beta = 50$, the method gives the optimal segmentation result.

4.6. Performance on simulated angiographic sequence

We evaluated our pipeline on a simulated sequence of 17 frames displaying CAs in 2D X-ray angiography under both respiratory and cardiac motions. The sequence was acquired with the XCAT software [26] that simulates both cardiac and respiratory mechanics including the motion of the diaphragm, heart, rib cage, and lungs. Ground truth segmentation mask of all the frames of the sequence is provided using the XCAT system. Results show that the proposed method succeeds in tracking and segmenting a right coronary artery within the entire 17 frames with a mean Dice coefficient of 0.98, precision of 0.99 and a recall of 0.97. Overall, the method succeeds in extracting and tracking the artery accurately despite its motion as illustrated in Fig. 17.

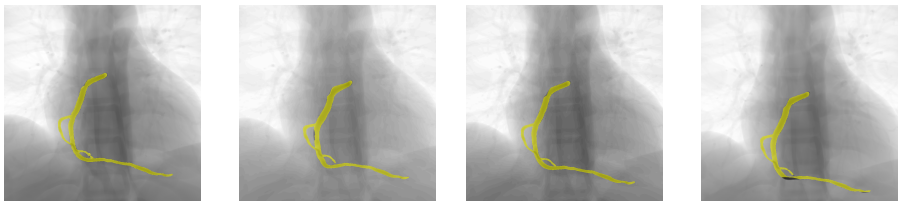

(a) Frame 1 (b) Frame 5 (c) Frame 10 (d) Frame 17

Figure 17: Results on simulated sequence: the segmentation result of the right coronary artery overlaid in yellow on frames 1, 5, 10 and 17.

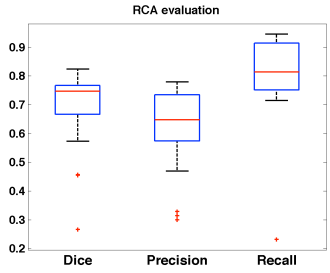

(a) RCA artery

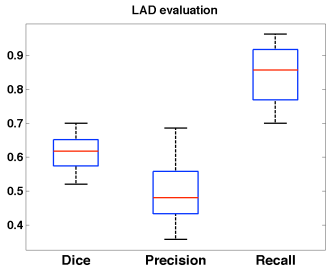

(b) LAD artery

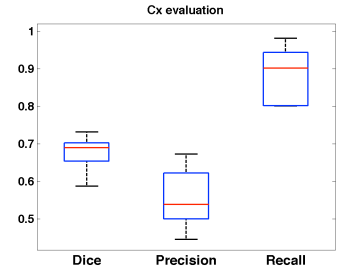

(c) Cx artery

Figure 18: Performance of the proposed pipeline depending on the nature of the coronary arteries.

4.7. Performance depending on the type of the vessel: RCA , LAD or Cx

This section evaluates the performance of the proposed algorithm in 3.3. The parameters' values were empirically selected following a K-fold cross validation. Optimal values used were $\alpha = 50$, $\beta = 1000$, and temporal parameter $\mu = 0.05$. Superpixel sizes for the SLIC [12] implementation are 20 and 10 (with a regularizer value of 0.01). Frangi's vesselness scales are within the range $[1, 8]$. Finally, $\gamma = 4000$ and $r = 1$ were selected for the adjacency matrix, and $\gamma_\tau = 50$ and $r_\tau = 1$ for the temporal adjacency matrix.

The performance of the proposed framework is assessed in tracking and extracting the vessel's lumen during the angiographic sequence. Because the motion range depends on the nature of the CA, we evaluated the dataset according to each category of CA (RCA, LAD, or LCX). Figure 18 shows the dependence of the performance on the nature of the artery in terms of Dice, precision, and recall values. Figure 19 shows the segmentation results at different frames in different sequences shown from top to bottom: LAD,

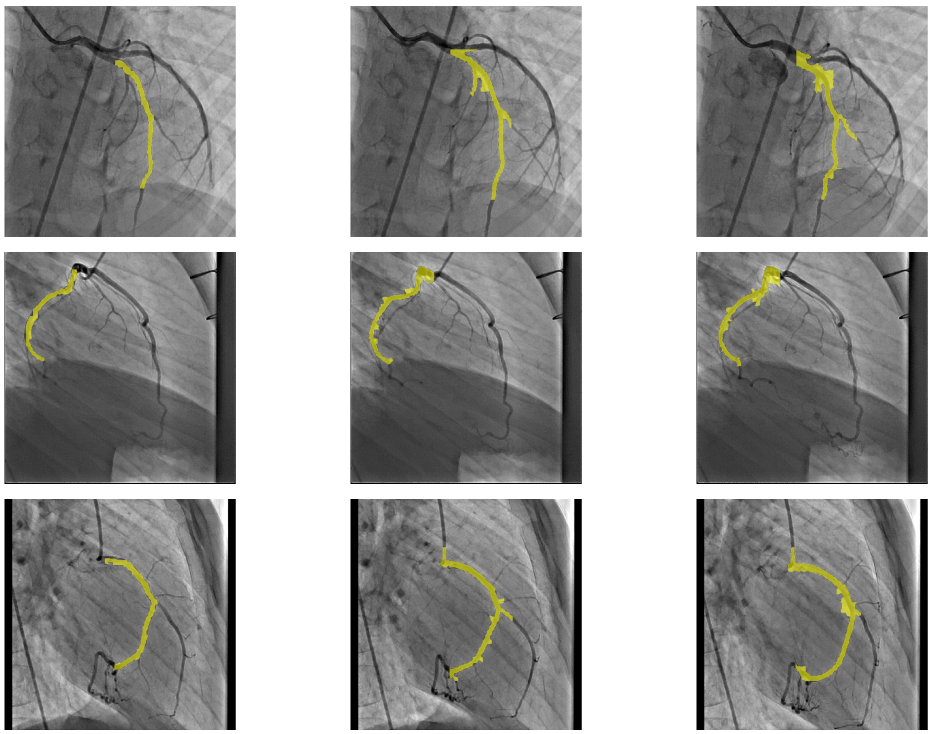

Figure 19: Segmentation mask overlaid in yellow on the original frames of three sequences at different times. Top row: result on LAD artery. Second row: result on a Cx artery. Third row: result on an RCA artery.

Cx, and RCA artery. The method gives the best performance when tracking RCA, with a Dice close to 0.8. Segmenting and tracking Cx arteries is more challenging, but there is still a good trade-off between the precision and recall with a mean Dice close to 0.7 and a high recall of 0.9. LAD arteries are the most challenging cases because of their nature in terms of their shape and motion. This leads to a mean Dice for LAD cases of 0.6, yet with a high recall value of 0.8.

5. Discussion

The proposed method preforms accurate segmentation and tracking of a CA in 2D X-ray angiography. The method is applied without any pre-processing to deal with the respiratory motion or cardiac motion, as shown in existing works [9, 8]. The proposed Temporal Vessel Walker with superpixels

(SP-TVW) is defined as the combination of a temporal prior with intensity and topological features. In addition, superpixels are used to regroup similar pixels, which leads to accurate and fast computations. Experimental tests on datasets of young patients show the efficiency and robustness of the proposed algorithm.

Table 3 highlights the contribution of the proposed SP-TVW compared to the previous iterations of the Temporal Vessel Walker method. While the use of the TVW pixelwise can track the artery, in some cases, it highlights the background noise as part of the vessel. On the other hand, applying the TVW in the multiscale framework limits the effect of noise. However, this can lead to the loss of contrast (especially at small scales), making the final segmentation result limited with low recall values. SP-TVW returns the highest trade-off between recall and precision values. The addition of superpixels contributes to the retrieval of similar groups of pixels from one frame to the next in a more accurate way than the application of TVW in a pixelwise fashion.The use of superpixels better highlights the difference between the foreground and background regions, as shown in Fig.9.

Previous studies have considered the tracking of CAs in 2D X-ray sequences. However, they either track manually selected seeds [9] without handling the respiratory motion of the arteries, or they extract the entire CA tree [3] without focusing on tracking specific arteries. We compared our proposed algorithm with the polyline tracking method [8], which is a method that performs well, and which is still cited in the literature as a key reference for tracking specific CAs in moving sequences [9]. Besides, the method is formulated as a minimization problem on a constructed graph, which is similar to the proposed method. Fig. 8 shows that polyline tracking preserves the general shape of the artery. This is explained by the fact that the neighborhood search using polyline tracking is small. However, as the artery expands owing to the cardiac work, polyline tracking cannot capture some parts of the artery. We believe that this is caused by the length constraint in the polyline method.This constraint is not used in our method, which leads to better tracking of the artery in time, even when the artery is expanding. Moreover, the proposed method has a better overlap with the ground-truth compared to the polyline method. Indeed, our method uses prior information from the previous frame, and also relies on the actual frame's information. Therefore, the proposed method is able to extract the centerline and track it accurately in the sequence. As illustrated in Table 2, our proposed work has a better quantitative performance in terms of its ability to find and track the

centerline of the vessel. Moreover, it has fewer errors in terms of localizing the centerline, which is crucial in order to compute properties of the artery such as its diameter or length.

The proposed method is based on different parameters, the most important of which are α, β, and μ from Eq. (8), and the superpixel size (SPsize). Figure 11 shows the importance of selecting the appropriate SPsize, especially in the case of thin, long structures such as CAs. When the SPsize is too small, the algorithm has a high precision, generating fewer false positive errors. However, a small SPsize leads to low recall values. The selection of the optimal superpixel size is important to maintain the balance between high recall and precision values. In addition, one CA may have a thick diameter at the proximal part of the artery and a thinner diameter at the distal part of the artery (as shown in Fig.7); hence, the proposed method computes the SP-TVW at different superpixel sizes to optimize the trade-off between the precision and recall, guaranteeing a better performance.

The results in Figure 15 indicate that having a μ value close to 1 helps the method in tracking the structure of interest, while being more robust to background noise. If $\mu = 10$ the method gives more weight to the last term in equation (8). Therefore, the segmentation is computed based on the prior information without considering the present frame's features. It is important to select the optimal value for μ, thus increasing the accuracy of the method used to track the artery, while remaining robust to background noise.

Fig. 16 shows that an optimal choice between α and β values leads to an optimal trade-off between recall and precision. Therefore, their values should be selected depending on the nature of the dataset.

Because each type of CA has a different shape and motion, we evaluated the dataset according to the different categories of CAs (RCA, LAD, and LCX). As shown in Figures 18 and 19, the proposed method has the best performance when tracking RCA. The RCA is one of the arteries that have a large range of motion during cardiac work. Despite the motion, the proposed method is able to track and extract the artery accurately. While the segmentation and tracking of Cx arteries is more challenging, it still allows a good trade-off between precision and recall. LAD arteries are the most challenging cases because of their shape. In fact, in all of the sequences displaying LAD, there is a vessel overlap or vessels that bifurcate from the main artery. Tracking LAD becomes more challenging as it is difficult to distinguish between the arteries. Therefore, in such cases, more features must be added to enhance the proposed method.

Overall, the proposed method shows a high recall value for all different types of coronary arteries. However, the proposed method can be sensitive to different factors, such as the presence of overlapping vessels and the low frame rate (15 fps). Despite these limitations, the proposed method produces encouraging results in enabling accurate tracking of the VOI and extracting its lumen. However, more work is necessary to enhance the precision of the proposed method by adding new features, such as the vessel's orientation.

6. Conclusion

This work presents a spatio-temporal algorithm for the simultaneous segmenting and tracking of a CA in a 2D X-ray moving sequence based on the Temporal Vessel Walker and superpixels (SP-TVW). The model combines temporal prior and intensity and topological features. The superpixels method regroups similar pixels together, which leads to the accurate extraction of thinner and thicker parts of the same artery and fewer computations.

Experimental tests on a dataset for young patients show the efficiency and robustness of the proposed algorithm, while dealing with respiratory and cardiac motions. The results of the proposed pipeline show that it is possible to build a model for the simultaneous tracking and segmenting of a vessel. The ability to accurately track a specific artery (or part of an artery) may be crucial for measuring the properties of the vessel during the cardiac cycle as well as helping with the detection of pathologies.

Future work includes using not only the previous frame's result but also the following frame as a prior to segment the current frame. It includes also the development of an adaptive formulation to automatically select the parameters of the proposed method depending on the contrast level in the X-ray sequence. Moreover, additional features are needed, such as the vessel's direction, to solve the challenge of overlapping vessels. Finally, more tests with longer sequences at different cardiac cycles will help to evaluate the repeatability of the proposed method.

7. Acknowledgment

The authors would like to thank the medical team at Sainte Justine Children hospital for their support in acquiring data. In particular, we thank Dr. Philippe Adjagba, Dr. Mohamed Bakloul, Ms. Denise Turnblom, Ms. Julie Lebrun, and Ms. Helene Sabourin. This research was funded by the Fonds

de recherche du Quebec Nature et technologies and the Natural Sciences and Engineering Research Council of Canada. A special thanks to Rémi Martin, Lou Hammel, Anh Thu Hang Vo and Binh Phan Tran.

8. References

[1] M. T. Tomkowiak, A. N. Raval, M. S. Van Lysel, T. Funk, M. A. Speidel, Calibration-free coronary artery measurements for interventional device sizing using inverse geometry x-ray fluoroscopy: in vivo validation, Journal of Medical Imaging 1 (3).

[2] J. P. Janssen, A. Rares, J. C. Tuinenburg, G. Koning, A. J. Lansky, J. H. Reiber, New approaches for the assessment of vessel sizes in quantitative (cardio-) vascular x-ray analysis, The international journal of cardiovascular imaging 26 (3) (2010) 259–271.

[3] C. Compas, T. Syeda-Mahmood, P. McNeillie, D. Beymer, Automatic detection of coronary stenosis in x-ray angiography through spatio-temporal tracking, in: Biomedical Imaging (ISBI), 2014 IEEE 11th International Symposium on, 2014, pp. 1299–1302.

[4] R. Liao, L. Duong, Y. Sun, K. Kirchberg, 3-d reconstruction of the coronary artery tree from multiple views of a rotational x-ray angiography, The International Journal of Cardiovascular Imaging 26 (7) (2010) 733–749.

[5] X. Ren, J. Malik, Learning a classification model for segmentation, in: ICCV, IEEE, 2003, pp. 10–17.

[6] F. M'hiri, N. Hoang, L. Duong, M. Cheriet, Hierarchical segmentation and tracking of coronary arteries in 2d x-ray angiography sequences, in: ICIP, 2015, pp. 1707 – 1711.

[7] D. Lesage, D. Angelini, I. Bloch, F.-L. G., A review of 3D vessel lumen segmentation techniques: Models, features and extraction schemes, Medical Image Analysis 13 (6) (2009) 819 – 845, includes Special Section on Computational Biomechanics for Medicine.

[8] M.-P. Dubuisson-Jolly, C.-C. Liang, A. Gupta, Optimal polyline tracking for artery motion compensation in coronary angiography, in: ICCV, IEEE, 1998, pp. 414–419.

[9] Y. Gao, H. Sundar, Coronary arteries motion modeling on 2D x-ray images, in: SPIE Medical Imaging, 2012, pp. 83161A–83161A.

[10] S. Ding, M. I. Miga, T. Pheiffer, A. L. Simpson, R. C. Thompson, B. M. Dawant, Tracking of vessels in intra-operative microscope video sequences for cortical displacement estimation, TBME 58 (7) (2011) 1985–1993.

[11] S. Laguitton, C. Boldak, C. Toumoulin, Temporal tracking of coronaries in multi-slice computed tomography, in: EMBS, IEEE, 2007, pp. 4512–4515.

[12] R. Achanta, A. Shaji, K. Smith, A. Lucchi, P. Fua, S. Susstrunk, Slic superpixels compared to state-of-the-art superpixel methods, TPAMI 34 (11) (2012) 2274–2282.

[13] C. Çiğla, et al., Efficient graph-based image segmentation via speeded-up turbo pixels, in: ICIP, IEEE, 2010, pp. 3013–3016.

[14] C. Desrosiers, Unsupervised segmentation using dynamic superpixel random walks, in: ICIP, 2015, pp. 1772 – 1776.

[15] F. M'hiri, L. Duong, C. Desrosiers, M. Cheriet, Vessel Walker: Coronary arteries segmentation using random walks and hessian-based vesselness filter, in: ISBI, 2013, pp. 918–921.

[16] L. Grady, Random walks for image segmentation, TPAMI 28 (11) (2006) 1768–1783.

[17] L. Grady, Multilabel random walker image segmentation using prior models, in: CVPR 2005, Vol. 1, 2005, pp. 763–770.

[18] A. Frangi, W. Niessen, K. Vincken, M. Viergever, Multiscale vessel enhancement filtering, MICCAI98 (1998) 130.

[19] A. K. Sinop, L. Grady, A seeded image segmentation framework unifying graph cuts and random walker which yields a new algorithm, in: ICCV 2007, IEEE, 2007, pp. 1–8.

[20] N. Otsu, A threshold selection method from gray-level histograms, IEEE Transactions on Systems, Man and Cybernetics 9 (1) (1979) 62–66.

[21] M. Freiman, L. Joskowicz, N. Broide, M. Natanzon, E. Nammer, O. Shilon, L. Weizman, J. Sosna, Carotid vasculature modeling from patient ct angiography studies for interventional procedures simulation, IJCARS 7 (5) (2012) 799–812.

[22] E. W. Dijkstra, A note on two problems in connexion with graphs, Numerische Mathematik 1 (1) (1959) 269–271.

[23] A. Hernández-Vela, C. Gatta, S. Escalera, L. Igual, V. Martin-Yuste, M. Sabaté, P. Radeva, Accurate coronary centerline extraction, caliber estimation, and catheter detection in angiographies, Information Technology in Biomedicine, IEEE Transactions on 16 (6) (2012) 1332–1340.

[24] A. J. Viera, J. M. Garrett, et al., Understanding interobserver agreement: the kappa statistic, Fam Med 37 (5) (2005) 360–363.

[25] S. Bouix, K. Siddiqi, A. Tannenbaum, Flux driven automatic centerline extraction, Medical Image Analysis 9 (3) (2005) 209–221.

[26] W. P. Segars, B. M. Tsui, Mcat to xcat: The evolution of 4-d computerized phantoms for imaging research, Proceedings of the IEEE 97 (12) (2009) 1954–1968.